Rapid self-assembly of brush block copolymers to photonic crystals

Benjamin R. Sveinbjörnsson[a,1], Raymond A. Weitekamp[a,b,1], Garret M. Miyake[a], Yan Xia[a], Harry A. Atwater[b], and Robert H. Grubbs[a,2]

[a]Arnold and Mabel Beckman Laboratories for Chemical Synthesis, Division of Chemistry and Chemical Engineering, California Institute of Technology, Pasadena, CA 91125; and [b]Thomas J. Watson Laboratories of Applied Physics, California Institute of Technology, Pasadena, CA 91125

Contributed by Robert H. Grubbs, July 30, 2012 (sent for review July 3, 2012)

The reduced chain entanglement of brush polymers over their linear analogs drastically lowers the energetic barriers to reorganization. In this report, we demonstrate the rapid self-assembly of brush block copolymers to nanostructures with photonic bandgaps spanning the entire visible spectrum, from ultraviolet (UV) to near infrared (NIR). Linear relationships were observed between the peak wavelengths of reflection and polymer molecular weights. This work enables "bottom-up" fabrication of photonic crystals with application-tailored bandgaps, through synthetic control of the polymer molecular weight and the method of self-assembly. These polymers could be developed into NIR-reflective paints, to combat the "urban heat island effect" due to NIR photon thermalization.

The rich morphologies afforded by the self-assembly of block copolymers (BCPs) yield versatile hybrid materials with diverse applications (1), such as lithographic templates (2), solid electrolytes (3), and photonic crystals (PCs) (4). When the domain periodicities of typical copolymer structures reach hundreds of nanometers, the effective optical lengths of the domains approach visible wavelengths. The resulting periodic modulation of the dielectric function can yield a photonic bandgap near the visible; within this gap, there are no allowed frequencies at which light can propagate through the material (5). The one-dimensional case, consisting of a stack of alternating layers, is termed a dielectric (or Bragg) mirror. This simple architecture forms the basis for a variety of modern optical elements, including filters, antireflection coatings, and resonant cavities. Recently, very high molecular weight block copolymers have enabled chemically and mechanically tunable PCs at visible frequencies (4, 6–8), providing a versatile platform for the development of unique nanostructures with exciting possibilities for functional, moldable, and paintable PCs.

For many applications, such as dielectric mirrors, broadband reflection is a requirement. Typically, this is accomplished by employing materials with high refractive index contrast (9). Size dispersity in multilayer structures offers another approach to broadband reflection. In this way, the inherent dispersity in self-assembled systems can be employed advantageously. In this report, we demonstrate broadband reflection into the NIR with two low-index materials, with a refractive index contrast of approximately 0.1. Because self-assembly methods easily provide dozens to hundreds of layers, a reflection coefficient of unity can, in principle, be obtained. To realize truly paintable photonic crystals, self-assembly must occur rapidly, with little or no processing, to yield dry, robust ordered nanostructures. This future technology has many potential applications, for example as photonic cladding for telecommunications fibers and NIR reflective paints. These photonic paints could be employed as surface coatings to improve energy efficiency in urban environments, combating the "urban heat island effect" by reflecting infrared radiation that would otherwise thermalize.

Traditionally, PCs have been fabricated using "top-down" techniques such as layer-by-layer stacking (10), electrochemical etching (11), multibeam holography (12), and phase mask lithography (13). These techniques offer the advantage of precision but require complex apparatuses and many processing steps. Colloidal assembly represents a "bottom-up" approach to PC fabrication (14, 15), although it is generally limited to face-centered cubic geometries. While colloidal templating is rapid and inexpensive, infilling with high refractive index inorganic materials is usually required to access a full photonic bandgap (14, 15). BCP nanostructures offer an attractive solution because they can be prepared from commodity chemicals and synthetically tuned to yield a wide range of geometries and functionalities with unique chemical, mechanical, and optical properties.

The typically slow and complex self-assembly of BCPs inhibits their ability to assemble to domain sizes large enough to reflect long wavelengths of visible light. The primary antagonist to self-assembly is chain entanglement—a defining characteristic of polymers, which significantly impedes high molecular weight (MW) polymers from achieving large, ordered domains. Reaching domain spacings beyond 100 nm is a significant challenge for BCPs (16–18) because the entanglement of high MW polymers presents a large kinetic barrier, despite the large thermodynamic driving force to microphase segregation. As a result, high MW BCPs often end up in a kinetically trapped state; equilibration is prohibited at a practical time scale. To overcome the practical limitations to the domain sizes and refractive indices of typical BCPs, assembled nanostructures are often swollen with additives, including small molecules (4, 6, 19), inorganic nanoparticles (20), or other polymers (17) to achieve photonic bandgaps in the visible and NIR. Additionally, extreme annealing conditions have been used successfully to prepare PC films from BCPs (21). The complex annealing procedures and additives demanded by much of the work to date on polymer PCs represent a huge barrier to the practical implementation of BCPs as commercially viable optical elements. As chain entanglement presents a fundamental energetic barrier to the reorganization of high MW BCPs into large, ordered nanostructures, it is a logical focal point for the development of methods to surmount these limitations. In this report, we employ a nonlinear macromolecular architecture with significantly reduced entanglement, the brush copolymer (22, 23), to afford rapid self-assembly into photonic crystals with tunable reflection across the entire visible spectrum and into the NIR.

Brush copolymers with high MW, low polydispersity index (PDI), and complete side chain grafting remain challenging targets for synthetic polymer chemists. There are many approaches to these macromolecules, each with their own obstacles (24, 25). In the "grafting through" or macromonomer (MM) method, the side chain containing a terminal monomer is synthesized first and

Author contributions: R.A.W., Y.X., and R.H.G. designed research; B.R.S., R.A.W., G.M.M., and Y.X. performed research; B.R.S. contributed new reagents/analytic tools; B.R.S., R.A.W., G.M.M., Y.X., and H.A.A. analyzed data; and B.R.S., R.A.W., G.M.M., Y.X., H.A.A., and R.H.G. wrote the paper.

The authors declare no conflict of interest.

[1]B.R.S. and R.A.W. contributed equally to this work.

[2]To whom correspondence should be addressed, E-mail: rhg@caltech.edu.

This article contains supporting information online at www.pnas.org/lookup/suppl/doi:10.1073/pnas.1213055109/-/DCSupplemental.

subsequently polymerized to yield the resulting brush polymer (24, 26). This approach ensures complete grafting of a well-defined side chain on every backbone monomer unit; however, it requires an extremely robust polymerization mechanism to achieve high MW while maintaining control of the PDI (25). Our group has recently utilized ruthenium (Ru) mediated ring-opening metathesis polymerization (ROMP) as an efficient means to convert MMs to well-defined high MW brush polymers (22, 27–30). Brush BCPs prepared by this route were observed to spontaneously assemble into large ordered nanostructures (>100 nm) (28), which piqued our interest in applying this approach to photonic crystals.

Results and Discussion

The lactide (L) and styrene (S) based MMs employed in this study were synthesized from *exo*-norbornene functionalized initiators, suited for the ring opening polymerization of racemic L and the controlled radical polymerization of S. The MMs had similar MWs and narrow molecular weight distributions (MWDs) (L-MM: $M_n = 6.1 \times 10^3$ g/mol, PDI = 1.20; S-MM: $M_n = 5.7 \times 10^3$ g/mol, PDI = 1.02). More importantly, the advantageous characteristics (i.e., livingness, stability, functional group and steric tolerance) of Ru-mediated ROMP enable the sequential polymerization of the MMs to brush BCPs in high yields with controlled MWs and narrow MWDs (Fig. 1). The MW of the brush BCPs were controlled by the MM to Ru ratio, and ranged from 1.08×10^6 to 6.64×10^6 g/mol, while maintaining relatively narrow MWDs (PDI = 1.07–1.58) considering the ultra-high MWs, highlighting the robustness of ROMP. For this study, we targeted blocks with near equal weight ratios with the goal of achieving lamellar nanostructures (see *SI Appendix* for details).

After preparing a series of well-defined brush BCPs with a broad range of MWs, we investigated a number of simple self-assembly methods to yield thin, solid films. Our annealing methods included controlled evaporation from dichloromethane (DCM) and tetrahydrofuran (THF) solutions, before and after thermal annealing, as well as direct thermal annealing of the solid polymer powder under compression between two glass substrates. The drastic effect of the assembly method on the resulting nanostructures is most starkly visualized by a single brush BCP ($M_n = 2.94 \times 10^6$ g/mol), which appeared blue when cast from DCM, green when cast from THF, and red after thermally annealing the green film cast from THF (Fig. 1*C*). Quantitative reflection measurements were performed on a spectrophotometer equipped with an "integrating sphere" diffuse reflectance accessory (see *SI Appendix*). The reflection spectra confirm the large differences between samples prepared by different annealing procedures (Fig. 2*A*). For the sample shown in Fig. 2, the first (longest wavelength) peak of reflection shifts by hundreds of nanometers, depending on the method of film preparation. The difference in color is not due to residual solvent; the films are completely dry, and we did not observe any color change upon placing a sample in high vacuum for more than 50 hours.

Scanning electron micrograph (SEM) cross-sections were used to directly image the film morphologies to further investigate causes of the observed reflection spectra. Although the thermally annealed samples must be composed of larger domains than the films prepared via controlled evaporation (as suggested by the greater λ_{max}), we were curious as to why the film cast from DCM provided the markedly altered reflection spectra. SEM images provided insight into the self-assembly of the films from different techniques, clearly visualizing the polymer morphologies and domain sizes (Fig. 2 *B–E*). For this polymer, all of the films, except those prepared from DCM, showed the expected stacked lamellar morphology for symmetric BCPs. In the case of the film cast from DCM, a disordered morphology is observed in the SEM image. The evaporative self-assembly process is dictated by a number of factors, including the kinetics of evaporation, quality of solvent, S/L interaction parameters, as well as the energetics of the glass/polymer interface. For many samples, the degree of lamellar order decreased as a function of distance from the glass interface (see *SI Appendix*). For BCPs with approximately equal volume fractions, the lamellar morphology is the most thermodynamically stable, as it minimizes the interfacial surface energy between the two constituent polymers. THF afforded larger and better ordered domains than DCM, which we attribute to the fact that it is a good solvent for this copolymer system (31). In addition, its decreased volatility affords improved chain mobility: rearrangement occurs during evaporation, before the chains enter the glassy state once all solvent is removed. After thermal annealing, these samples become more ordered, with larger domain sizes, as observed in the SEMs and evidenced by the reflection spectra. Films that were directly thermally annealed from dry polymer powder also formed well-ordered lamellae with long wavelength reflection. The improved reflection coefficient is a consequence of film thickness.

We observed the first order peak of reflection to be a linear function of MW, for all of the self-assembly techniques employed. This is in contrast to a corresponding linear copolymer system, where the domain spacing is proportional to $MW^{0.81}$ (32). Because the peak wavelength and domain spacing are directly related by the equation $\lambda_{max} = 2(n_1x_1 + n_2x_2)$ (18), our results suggest that the brush BCPs studied yield a larger increase in domain spacing per monomer incorporated than a corresponding linear system. Given the high persistence lengths of these brush polymers (22), we rationalize this observation in terms of the

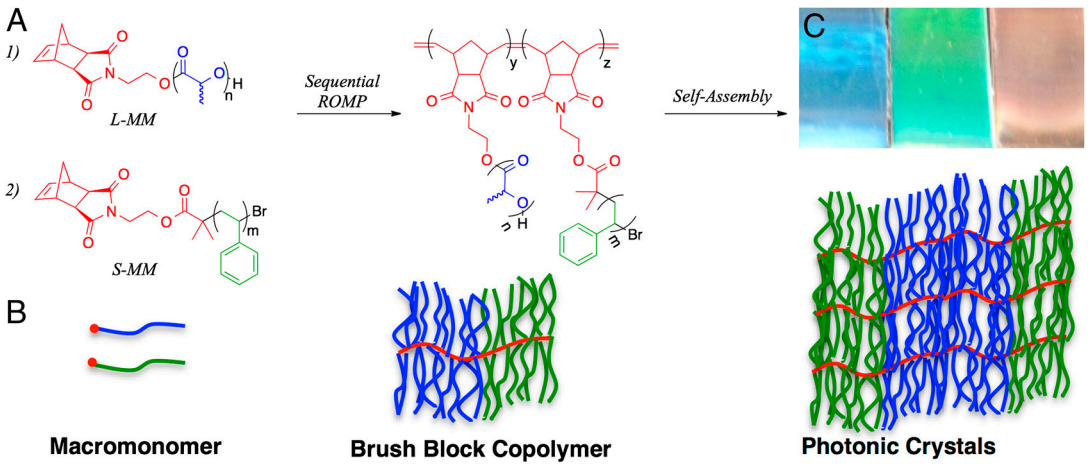

Fig. 1. (*A*) S- and L-based MMs were sequentially polymerized by ROMP to brush BCPs. (*B*) A schematic representation depicts the brush BCPs and their assembly into ordered lamellar nanostructures. (*C*) Different annealing techniques render unique PCs for the same polymer, as shown in this photograph.

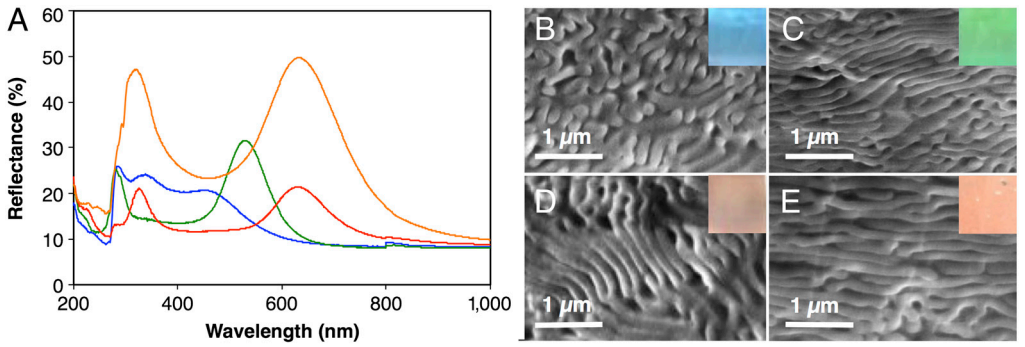

Fig. 2. (*A*) Reflection spectra are plotted for the brush BCP ($M_n = 2.94 \times 10^6$ g/mol) films prepared from the controlled evaporation from DCM (blue), or THF, before (green) and after (red) thermal treatment, as well as via thermal annealing under compression (orange). (*B*) SEM cross-sections reveal the morphology of the middle of the brush BCP films prepared from the controlled evaporation from DCM (*B*), THF before (*C*) and after (*D*) thermal annealing, as well as by direct thermal annealing under compression (*E*). The insets are photographs of the samples.

degree of backbone extension enforced by the steric congestion of the brushes. Thus, the brush polymer architecture enables both a large equilibrium scaling for self-assembled structures as well as a very fast equilibration rate, due to the significantly reduced chain entanglement (even at ultra-high MW).

Direct thermal annealing of the polymer powders under compression proved to be the most successful assembly technique, in that it enabled ultra-high MW polymers to reach ordered nanostructures with PC characteristics at NIR wavelengths (Fig. 3 *E* and *F*). By contrast, in the case of controlled evaporation, most of the high molecular weight polymers ($M_n > 3 \times 10^6$ g/mol) did not assemble into films with distinct Bragg reflection peaks. The unmatched structural order achieved through thermal annealing is highlighted by the fact that the ultra-high MW polymers possessed photonic bandgaps well into the NIR (up to $\lambda_{max} =$ 1311 nm), an unprecedented wavelength regime for unswelled BCP photonic crystals. Furthermore, the low energetic barriers to reorganization enable the application of any BCP self-assembly technique to our system, to achieve improved lamellar order and optical performance. As NIR dielectric mirrors, these robust solid state PCs enable a host of exciting applications for BCPs to telecommunications and thermal radiation management.

To justify the proposed mechanism of the observed reflection spectra, transfer matrix simulations (9) were employed to model the reflection spectra of the polymer photonic crystals. The complex refractive indices of each block were measured for the corresponding brush homopolymers by ellipsometry. The inputs to our script are: the frequency-dependent refractive indices, measured first order peak of maximum reflectance, number of layers approximated by SEM, and the weight fractions of each block measured by NMR (see *SI Appendix*). An initial guess of the size of each block domain was made using the first order peak of reflection, using the equation $\lambda_{max} = 2(n_1x_1 + n_2x_2)$, assuming equal polymer densities. To account for the increased bandwidth of the reflection peaks due to size dispersity and disorder in the nanostructure, two free parameters were introduced: coefficients of variation (CVs) for layer thickness and phase decoherence. Introducing partial phase decoherence in transfer matrix simulations has been previously demonstrated as a means of approximating interfacial roughness (33). A normal distribution of thickness and phase perturbation was used, averaged over 1000 simulations and smoothed to remove noise (see *SI Appendix* for modeling details).

The angle dependent reflection spectra of a well-ordered sample were measured and compared with one-dimensional transfer

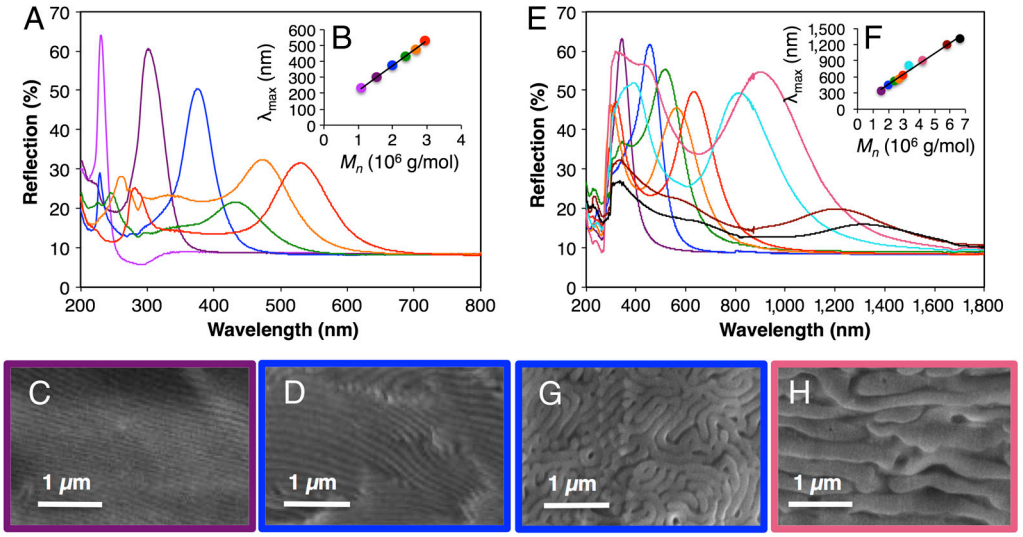

Fig. 3. (*A*) Reflectance is plotted as a function of wavelength for the films prepared from the controlled evaporation from THF for several different MW polymers. (*B*) λ_{max} is plotted against MW for films prepared from the controlled evaporation of THF. SEM cross-sections are shown for the middle of BCP films with $M_n = 1.53 \times 10^6$ g/mol. Linear fit $R^2 = 0.997$. (*C*) and $M_n = 1.99 \times 10^6$ g/mol (*D*) prepared from the controlled evaporation of THF. (*E*) Reflectance is plotted as a function of wavelength for the films prepared by thermal annealing under compression for several different MW polymers. (*F*) λ_{max} is plotted against MW for films prepared by thermal annealing under compression. SEM cross-sections are shown for the middle of BCP films with $M_n = 1.99 \times 10^6$ g/mol. Linear fit $R^2 = 0.984$. (*G*) and $M_n = 4.21 \times 10^6$ g/mol (*H*) prepared by thermal annealing under compression.

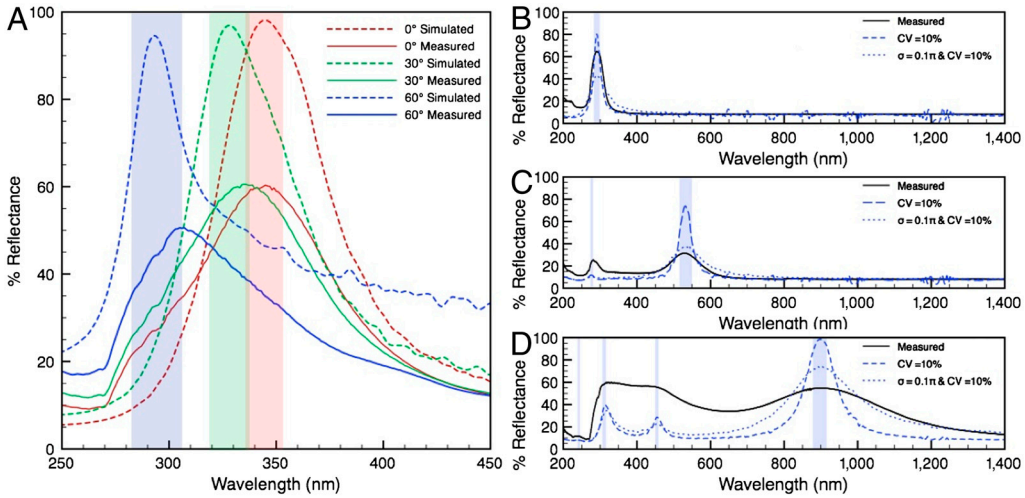

Fig. 4. (*A*) The angle-dependent reflection of a film thermally annealed under compression from a BCP with $M_n = 1.53 \times 10^6$ g/mol shows good agreement between the simulated (dashed, size CV = 10%, no decoherence) and measured (solid) spectra. Simulated (dashed, size CV = 10%, with and without partial decoherence) and measured (solid) reflection spectra of three different samples are shown: (*B*) $M_n = 1.53 \times 10^6$ g/mol, evaporated from DCM, (*C*) $M_n = 2.94 \times 10^6$ g/mol, evaporated from THF, (*D*) $M_n = 4.21 \times 10^6$ g/mol, thermally annealed under compression. The shaded areas represent the photonic bandgaps simulated for perfect alternating multilayers with no layer thickness dispersity.

matrix simulations. The angular frequency response shows good agreement between experiment and simulation (Fig. 4*A*). We attribute the difference in amplitude to the angular variation due to the curvature of the lamellae and the differences between the fitted and actual complex refractive indices. Additionally, simulations were run for three samples formed by three different assembly procedures, with different MWs representative of the full range of the series studied (Fig. 4 *B–D*). For our simulations, the CV for the layer thicknesses was chosen to be 10%, which we found to be large enough to demonstrate the effect of size distribution on the line widths of the optical spectra, while small enough to clearly resolve the higher order peaks. Partial phase decoherence further contributes to peak broadening, and is well rationalized considering the roughness observed by SEM (33). The qualitative features of the measured spectra are well represented in the simulations (Fig. 4). Our modeling strongly suggests that the observed lamellar nanostructures consist of alternating polymer layers, which represent pseudo-1D photonic crystals. Despite the moderate to poor lamellar alignment observed in the SEM cross-sections, our 1D transfer matrix simulations can qualitatively predict reflection spectra, enabling the design of optical components using this platform.

In conclusion, we have demonstrated rapid self-assembly of high molecular weight brush polymers as a facile method for generating ordered nanostructures with large domain sizes, specifically pseudo-1D photonic crystals. The reduced chain entanglement of brush BCPs enables assembly of large nanostructures that reflect long wavelength light without the use of any additives. The linear trend of λ_{max} as a function of MW enables one to synthetically "dial-in" dielectric mirrors with first order peaks spanning from the UV to NIR. We envision that materials produced through this approach have potential as NIR-reflecting building materials, to inhibit the thermalization of NIR radiation in urban environments. Moreover, the functional flexibility of our approach enables a host of new directions for functional, compliant and stimuli-responsive photonic elements.

ACKNOWLEDGMENTS. This work was supported by the NSF (CHE-1048404). R.A.W. was supported in part by the DOE "Light-Material Interactions in Energy Conversion" Energy Frontier Research Center (DE-SC0001293). R.A.W. thanks the Resnick Institute for a graduate fellowship. Reflection measurements were collected at the Molecular Materials Research Center of the Beckman Institute of the California Institute of Technology. We thank Zhen-Gang Wang for helpful discussions and Bryce Sadtler for assistance with the reflection measurements.

1. Bates FS, et al. (2012) Multiblock polymers: Panacea or Pandora's box? *Science* 336:434–440.
2. Segalman RA (2005) Patterning with block copolymer thin films. *Mater Sci Eng R Rep* 48:191–226.
3. Wanakule NS, Virgili JM, Teran AA, Wang Z-G, Balsara NP (2010) Thermodynamic properties of block copolymer electrolytes containing imidazolium and lithium salts. *Macromolecules* 43:8282–8289.
4. Kang Y, Walish JJ, Gorishnyy T, Thomas EL (2007) Broad-wavelength-range chemically tunable block-copolymer photonic gels. *Nat Mater* 6:957–960.
5. Joannopoulos JD (2008) *Photonic Crystals: Molding The Flow of Light* (Princeton University Press, Princeton, NJ).
6. Valkama S, et al. (2004) Self-assembled polymeric solid films with temperature-induced large and reversible photonic-bandgap switching. *Nat Mater* 3:872–876.
7. Ge J, Yin Y (2011) Responsive photonic crystals. *Angew Chem Int Ed* 50:1492–1522.
8. Runge MB, Bowden NB (2007) Synthesis of high molecular weight comb block copolymers and their assembly into ordered morphologies in the solid state. *J Am Chem Soc* 129:10551–10560.
9. Orfanidis SJ (2008) Electromagnetic waves and antennas., Available at http://www.ece.rutgers.edu/~orfanidi/ewa. Accessed March 19, 2012.
10. Lin SY, et al. (1998) A three-dimensional photonic crystal operating at infrared wavelengths. *Nature* 394:251–253.
11. Masuda H, et al. (1999) Photonic crystal using anodic porous alumina. *Jpn J Appl Phys* 38:L1403–L1405.
12. Campbell M, Sharp DN, Harrison MT, Denning RG, Turberfield AJ (2000) Fabrication of photonic crystals for the visible spectrum by holographic lithography. *Nature* 404:53–56.
13. Jeon S, et al. (2004) Fabricating complex three-dimensional nanostructures with high-resolution conformable phase masks. *Proc Natl Acad Sci USA* 101:12428–12433.
14. Braun PV, Wiltzius P (1999) Electrochemically grown photonic crystals. *Nature* 402:603–604.
15. Bertone JF, Jiang P, Hwang KS, Mittleman DM, Colvin VL (1999) Thickness dependence of the optical properties of ordered silica-air and air-polymer photonic crystals. *Phys Rev Lett* 83:300–303.
16. Rzayev J (2009) Synthesis of polystyrene–polylactide bottlebrush block copolymers and their melt self-assembly into large domain nanostructures. *Macromolecules* 42:2135–2141.
17. Urbas A, et al. (2000) Tunable block copolymer/homopolymer photonic crystals. *Adv Mater* 12:812–814.
18. Edrington AC, et al. (2001) Polymer-based photonic crystals. *Adv Mater* 13:421–425.
19. Parnell AJ, et al. (2011) Continuously tuneable optical filters from self-assembled block copolymer blends. *Soft Matter* 7:3721–3725.
20. Lee I, et al. (2010) Quasi-amorphous colloidal structures for electrically tunable full-color photonic pixels with angle-independency. *Adv Mater* 22:4973–4977.
21. Hustad PD, Marchand GR, Garcia-Meitin EI, Roberts PL, Weinhold JD (2009) Photonic polyethylene from self-assembled mesophases of polydisperse olefin block copolymers. *Macromolecules* 42:3788–3794.
22. Hu M, Xia Y, McKenna GB, Kornfield JA, Grubbs RH (2011) Linear rheological response of a series of densely branched brush polymers. *Macromolecules* 44:6935–6943.
23. Lee H, Matyjaszewski K, Yu-Su S, Sheiko SS (2008) Hetero-grafted block brushes with PCL and PBA side chains. *Macromolecules* 41:6073–6080.
24. Hadjichristidis N, Pitsikalis M, Pispas S, Iatrou H (2001) Polymers with complex architecture by living anionic polymerization. *Chem Rev* 101:3747–3792.

25. Neiser MW, Okuda J, Schmidt M (2003) Polymerization of macromonomers to cylindrical brushes initiated by organolanthanides. *Macromolecules* 36:5437–5439.
26. Heroguez V, Breunig S, Gnanou Y, Fontanille M (1996) Synthesis of α-norbornenylpoly (ethylene oxide) macromonomers and their ring-opening metathesis polymerization. *Macromolecules* 29:4459–4464.
27. Xia Y, Kornfield JA, Grubbs RH (2009) Efficient synthesis of narrowly dispersed brush polymers via living ring-opening metathesis polymerization of macromonomers. *Macromolecules* 42:3761–3766.
28. Xia Y, Olsen BD, Kornfield JA, Grubbs RH (2009) Efficient synthesis of narrowly dispersed brush copolymers and study of their assemblies: The importance of side chain arrangement. *J Am Chem Soc* 131:18525–18532.
29. Johnson JA, et al. (2011) Polymers by ROMP: Grafting-through and clicking-to. *J Am Chem Soc* 133:559–566.
30. Johnson JA, et al. (2010) Drug-loaded, bivalent-bottle-brush polymers by graft-through ROMP. *Macromolecules* 43:10326–10335.
31. Vayer M, et al. (2010) Perpendicular orientation of cylindrical domains upon solvent annealing thin films of polystyrene-b-polylactide. *Thin Solid Films* 518:3710–3715.
32. Zalusky AS, Olayo-Valles R, Wolf JH, Hillmyer MA (2002) Ordered nanoporous polymers from polystyrene-polylactide block copolymers. *J Am Chem Soc* 124:12761–12773.
33. Troparevsky MC, Sabau AS, Lupini AR, Zhang Z (2010) Transfer-matrix formalism for the calculation of optical response in multilayer systems: From coherent to incoherent interference. *Opt Express* 18:24715–24721.